


Reading magnetic ink patterns with magnetoresistive sensors

Cite as: AIP Advances **8**, 056633 (2018); <https://doi.org/10.1063/1.5007693>

Submitted: 02 October 2017 . Accepted: 19 November 2017 . Published Online: 09 January 2018

K. J. Merazzo , T. Costa, F. Franco, R. Ferreira, M. Zander, M. Türr, T. Becker, P. P. Freitas, and S. Cardoso



View Online



Export Citation



CrossMark

ARTICLES YOU MAY BE INTERESTED IN

[MnNi-based spin valve sensors combining high thermal stability, small footprint and pTesla detectivities](#)

AIP Advances **8**, 056644 (2018); <https://doi.org/10.1063/1.5007668>

[Barrier breakdown mechanism in nano-scale perpendicular magnetic tunnel junctions with ultrathin MgO barrier](#)

AIP Advances **8**, 055908 (2018); <https://doi.org/10.1063/1.5007656>

[Broadband voltage rectifier induced by linear bias dependence in CoFeB/MgO magnetic tunnel junctions](#)

Applied Physics Letters **112**, 252401 (2018); <https://doi.org/10.1063/1.5029363>

Don't let your writing
keep you from getting
published!

AIP | Author Services

Learn more today!



Reading magnetic ink patterns with magnetoresistive sensors

K. J. Merazzo,^{1,a} T. Costa,^{1,2} F. Franco,^{1,2} R. Ferreira,⁴ M. Zander,³ M. Türr,³ T. Becker,³ P. P. Freitas,^{4,1} and S. Cardoso^{1,2}

¹INESC - Microsistemas e Nanotecnologias, Rua Alves Redol, 9, Lisbon 1000-029, Portugal

²Instituto Superior Tecnico - Universidade de Lisboa, Lisboa, Portugal

³BOGEN Electronic GmbH, Potsdamer Straße 12-13, 14163 Berlin, Germany

⁴International Iberian Nanotechnology Laboratory (INL), 4715-31 Braga, Portugal

(Presented 10 November 2017; received 2 October 2017; accepted 19 November 2017; published online 9 January 2018)

Information storage and monitoring relies on sensitive transducers with high robustness and reliability. This paper shows a methodology enabling the qualification of magnetic sensors for magnetic pattern readout, in applications different than hard disk magnetic recording. A magnetic tunnel junction MTJ sensor was incorporated in a reader setup for recognition of the magnetization of patterned arrays made of CoCrPt thin films and magnetic ink. The geometry of the sensor (in particular, the footprint and vertical distance to the media) was evaluated for two sensor configurations. The readout conditions were optimized to cope for variable media field intensity, resulting from CoCrPt film or magnetic ink thickness, with fixed reading distance and dimensions of the pattern. The calibration of the ink magnetic signal could be inferred from the analytical calculations carried out to validate the CoCrPt results. © 2018 Author(s). All article content, except where otherwise noted, is licensed under a Creative Commons Attribution (CC BY) license (<http://creativecommons.org/licenses/by/4.0/>). <https://doi.org/10.1063/1.5007693>

Nowadays electronic application requirements force us to explore new solutions in order to satisfy the huge hunger for new functional devices. These are often required to control different measurable magnitudes in the micrometer range and measurement resolutions in the nanometer range. Security and industrial areas have found a good solution on magnetic ink solving many issues that other systems deal with, but at the same time brings the need to develop magnetic sensors especially for it. In this work we show magnetic measuring techniques based on magneto-resistive (MR) technology that has been developed in order to read magnetic ink composed of magnetic particles and CoCrPt media. The later is largely used in magnetic tape technology for recording,¹⁻³ prepared by sputtering as part of a multilayer system, where very specific processes are used in order to improve the crystal orientation, the impurities levels and the magnetic properties.³ Meanwhile, TMR sensors are the new alternative,^{1,4} substituting the GMR sensors,⁵ for the reading part, thanks to their good sensitivity and high signal output.⁶ The presented work makes an approach to the reading techniques instead that recording technique, since the progresses achieved on thin film magnetic tapes open a realm of opportunities for high resolution, high sensitivity sensors as TMR.

The aim of this work is to find the best sensor configuration to read the magnetic signal created by a magnetic ink pattern. This ink is composed of magnetic particles in a solvent matrix, printed with different thicknesses over normal paper. To avoid clustering of the magnetic particles, the ink formulation is paramagnetic, therefore an external magnetic field is needed to magnetize it during the measurements. This study was done with two different sensors configuration and their validation was done by experimental and analytical studies of a CoCrPt thin film patterned array.

^aemail of the corresponding author: kmerazzo@inesc-mn.pt

A series of sensors were developed based on the stack: $[\text{Ta } 5/\text{CuN } 25] \times 6/\text{Ta } 5/\text{Ru } 5/\text{Ir}_{24}\text{Mn}_{76} 20/\text{Co}_{70}\text{Fe}_{30} 2/\text{Ru } 0.85/\text{Co}_{40}\text{Fe}_{40}\text{B}_{20} 2.6/\text{MgO } 1/\text{Co}_{40}\text{Fe}_{40}\text{B}_{20} 2/\text{Ta } 0.21/\text{Ni}_{81}\text{Fe}_{19} 4/\text{Ru } 0.20/\text{Ir}_{24}\text{Mn}_{76} 6/\text{Ru } 2/\text{Ta } 5/\text{Ru } 10$ (thicknesses in nanometer, target material composition in at.%), with resistance-area product of $20 \text{ k}\Omega \mu\text{m}^2$, deposited in a Singulus Timaris sputtering tool at INL, on a thick silicon wafer covered with $1 \mu\text{m}$ SiO_2 layer. Magnetic tunnel junction (MTJ) based sensors were then microfabricated at INESC-MN by a combination of lithography (DWL) and etching (Nordiko 3600) patterning techniques.⁷ Two different sensors were used: 1) Sensor #1 (S1) composed of 72 MTJs structures with a single area of $50 \times 50 \mu\text{m}^2$, connected in series and disposed in a 9×8 matrix ($500 \times 500 \mu\text{m}^2$) to maximize the signal to noise ratio (SNR);⁸ 2) Sensor #2 (S2) consists on one line of 4 MTJs with single area of $10 \times 4 \mu\text{m}^2$, connected in series with in a total spatial area of $59 \times 4 \mu\text{m}^2$, which is expected to have more accuracy on the reading distance (RD); a schematic drawing of both sensors configuration are presented in Figure 1(a). After processing, an optimized sequence of two consecutive annealing steps at different temperatures for each AFM layer (each IrMn has different blocking temperature due to the different thicknesses) were performed to set the free layer perpendicularly to the pinned layer and achieve a linear response.^{1,9} The direction of the pinned layer magnetization was set in order to fabricate a sensitive device capable to detect the magnetic field component perpendicular (B_z) to the surface plane of the magnetic materials under test. The sensor chips have been then diced and wire-bonded onto a rigid printed circuit board. Finally, a set of permanent magnets (NdFeB, dimensions $10 \times 4 \times 1 \text{ mm}$, 1.40-1.46 T of remanent magnetization) were mounted at a distance of 3 mm of the sensor chip (6mm between them), to create a magnetic field for ink saturation. Figure 1(b) and (c) shows the geometry used for the sensor setup and patterned ink.

Upon packaging, the sensors magneto-transport curves ($R(H)$)¹⁰ were obtained under an uniform external magnetic field along the sensing direction (z axis), as shown in Figure 1(e) and (f). Sensor S1 has a 534Ω resistance, a tunneling magnetoresistance (TMR) of 131% - which is limited by contact resistance due to a high number of MTJs connected in series, and a linear response within a $\pm 2 \text{ mT}$ range and non-hysteretic behavior (0.12 mT coercivity, H_c). Through an effective crossed configuration between the free and pinned layer magnetization, a high sensitivity of 1.51 V/T is achieved under a current of $10 \mu\text{A}$ across the array. Sensor S2 has an 1161.3Ω resistance, a

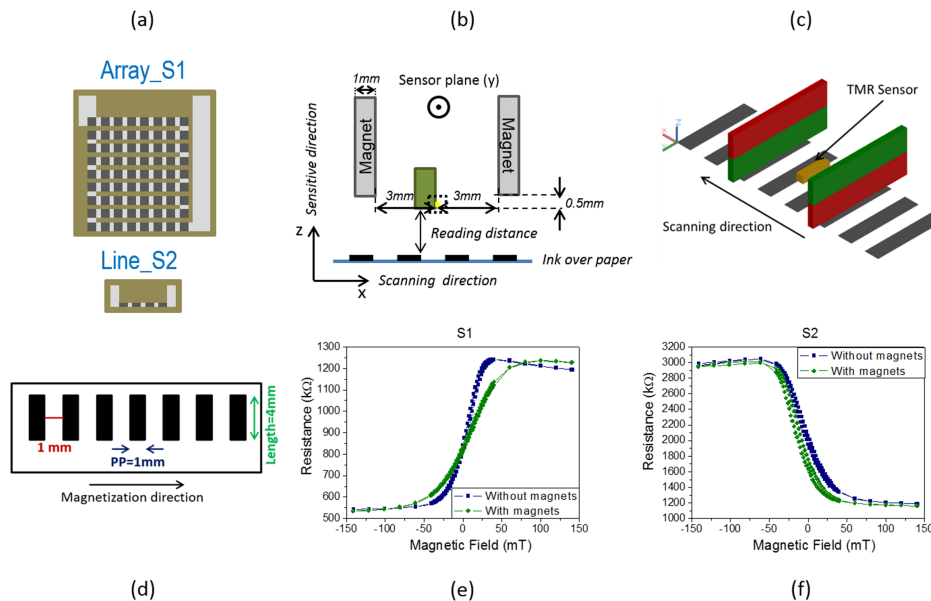


FIG. 1. (a) Distribution of 72 MTJ elements in an array (sensor S1), and 4 MTJ elements forming one row or line (sensor S2); (b) and (c) MR sensor geometry with poles configuration of the magnet; sensor and magnets position; (d) top view schematic drawing of the magnetic patterns and (e) and (f) transfer curves of the S1 and S2, respectively, with and without the permanent magnets.

TMR of 159.5 % and a linear response within a ± 2 mT range and a coercivity of 0.2 mT. The sensitivity is 26.4 V/T under a current of 100 μ A across the row. The impact of the permanent magnets in the vicinity of the chip was assessed and an optimal configuration could lead to still high sensitive linear curves, with sensitivity of 0.76 V/T and 28.4 V/T for S1 and S2, respectively. In the former, the sensitivity has decreased in 50 % but on S2 has increased slightly (see Figure 1(e) and 1(f)).

In order to compare with the printed ink, a 100nm thick CoCrPt film (remanent magnetization $M_r = 580$ kA/m and $H_c = 133.5$ kA/m, MH shown in Figure 2(a)) was deposited in an Alcatel SCM 450 sputtering system, and patterned by ion beam milling (Nordiko3600 system) onto rectangular element arrays with the same dimensions as the printed ink (1 mm x 4 mm), Figure 1(d) and Figure 2(a). This has allowed to check the B_z magnetic field component collected by the sensors, and compared directly with the values obtained by analytical calculations. The magnetic field produced by a magnetized media with a well-defined and constant magnetization ($\nabla \cdot \vec{M} = 0$) is computed using Eq. (1):

$$\vec{H}(\vec{r}) = \frac{1}{4\pi} \int_S d^2r' \hat{n}' \cdot \vec{M}(\vec{r}') \frac{\vec{r} - \vec{r}'}{|\vec{r} - \vec{r}'|^3}, \quad (1)$$

where \vec{r}' is the vector position to the field source while \vec{r} is the vector position to the point where the magnetic field is computed. The unit vector \hat{n}' is the outward surface normal at \vec{r}' .¹¹ Since the magnetic field at the middle of the magnetic pattern is measured by a micrometric magnetoresistive sensor with a nanometric thickness, its dimension is negligible according to the pattern length. Therefore, the magnetic field along the z axis can be simulated at the position $\vec{r} = (x, z)$ (where x is the scanning direction and z the out of plane axis) considering a 2D approach of (1):

$$H_z(\vec{r}) = -\frac{M_r}{2\pi} \ln \frac{r_2}{r_1}, \quad (2)$$

where M_r is the remanent magnetization (magnetization at zero field), while r_1 and r_2 are the distances from the upper and lower surface end points to the point (x, z) . Figure 2(b) shows a 2D approximation of the system under study, which comprises a set of N magnetic elements (ink patterns or magnetic CoCrPt) spaced by a distance equal to their width.

Consequently, the magnetic field produced by this periodic pattern of N cells can be simulated at a point (x, z) by taking into account the sum of the contributions of each cell:

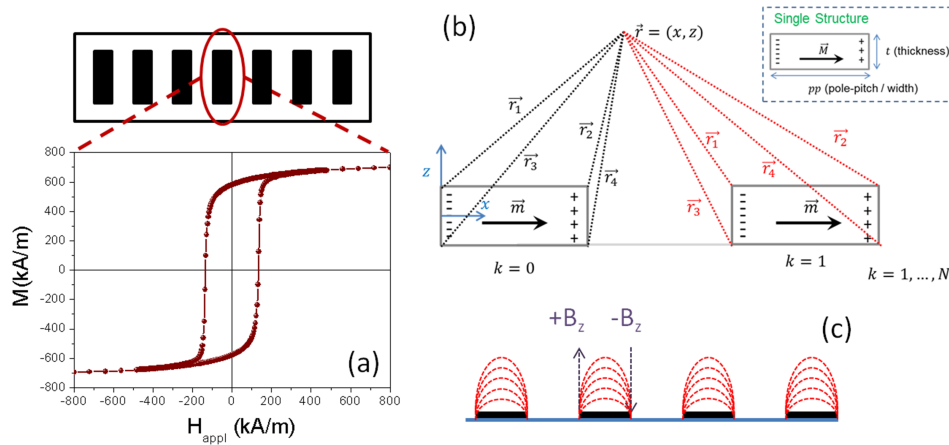


FIG. 2. (a) CoCrPt pattern as in Figure 1b and the MH of one unit of the pattern (b) Cross section view of the 2D model approximation of the system under study with N patterned CoCrPt elements (thickness t, along z) spaced by their width along the scanning direction (x axis). (c) Cross section profile of the stray field or B_z component produced by the magnetic media (B_z is exaggeratedly large for demonstrative purposes).

$$H_z(x, z) = \frac{M_s}{2\pi} \sum_{k=0}^{N-1} \left(-\ln \frac{r_2}{r_4} + \ln \frac{r_1}{r_3} \right). \quad (3)$$

Despite a micrometric dimension, the magnetic field measured by the magnetoresistive sensor is a result of an average field over its sensing area, which implies an integration of Eq. 3 across the sensor dimension, resulting in a lower magnetic field output when the sensor area is similar or larger than the CoCrPt pattern (CoCrPt media).

The magnetic ink (ink media) has been printed on normal paper with a pattern composed of a series of rectangles with a width or pole pitch (PP) of 1 mm, the distance between them is the same as the PP (1 mm), length of 4 mm and variable thickness of the order of microns, Figure 1(d), which is represented by the amount of printed layers, L (one over the other). The selected thicknesses of the magnetic ink are: 1L, 2L, 3L and 5L. The magnetic characterization of the ink printed over paper was done in a DSM 880 Vibrating Sample Magnetometer (VSM), where the hysteresis loops (MH) were obtained. The MR sensor setup for the ink and CoCrPt media B_z component measurements is composed of an automated XYZ scanner with a micrometric resolution and a set of electronic instruments to generate the required signals and to demodulate the probe output. All the details of the scanner set-up can be found in Ref. 12.

The experiment consists in a direct output signal from S1 or S2 of the media. The scanning of the sensor over the media was made at a constant RD, in this case 500 μm , which corresponds to half of the PP, Figure 1(b). The magnetization of the CoCrPt media during the scanning lies on the plane of the paper thanks to the external magnetic field applied by the two permanent magnets, which is approximately 70 mT, causing at the short edges of the rectangles uncompensated magnetic poles or stay fields in the z direction, Figure 2(c), which are the ones detected by the sensors. Figure 3(a) shows the experimental results and the simulations for CoCrPt media, by both sensors. These measurements represent a z-magnetic field component of approximately $11.1 \pm 0.9 \mu\text{T}$ and $25.8 \pm 2.3 \mu\text{T}$, obtained from S1 and S2, respectively; Figure 3(b) shows the schematics rectangles of the pattern overlapping the corresponding B_z , to illustrate the different positions of the amplitudes. We obtained lower amplitude from S1 as expected (S1 signal is the 43% of the signal obtained by S2), while the signal-to-noise ratio (STN) is similar on both sensors. The variation of B_z decreases with the RD, and since S1 is composed of a matrix of 72 MTJs of 8 rows (each row with 9 MTJ distributed in the X-direction), each one with a different RD resulting in different amplitude (bigger RD, smaller signal); as the MTJs inside a sensor are connected in series, the signal obtained for each sensor is computed as the sum of the individuals MTJs signal, i.e. the magnetic field measured by the magnetoresistive

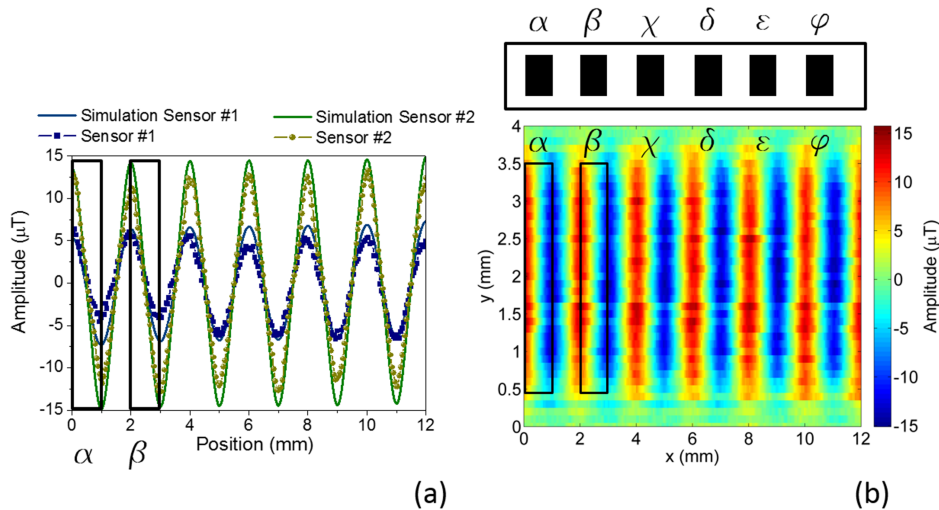


FIG. 3. CoCrPt: (a) Magnetic signal and simulations for S1 and S2 along the center of the pattern; (b) Experimental 2D Magnetic scanning with S2. Inside the amplitude vs. position curves and the magnetic scanning, we can observe a schematic drawing of the patterns for demonstration purposes.

sensor is a result of an average field over its sensing area resulting in a lower magnetic field output (as explained before). An advantage of measuring the average of such many elements is that we have a higher SNR, smoothing the curve in a very good way. The difference with S2 is that the average is done only between 4 MTJs elements at the same height, giving a more accurate value of the real amplitude. Also a noisy signal was expected since the average is done only between 4 elements; but this is not the case, which demonstrates the good performance of the sensor. Figure 3(b) shows a 2D scanning of the CoCrPt media; here we can see how the scanning process has a very good spatial resolution of the B_z component produced by the pattern. Inside the graph of amplitude vs. position curves, Figure 3(a), and the magnetic scanning, Figure 3(b), we can observe a drawing of the patterns (4 mm x 1 mm) with the purpose to demonstrate how the uncompensated poles are distributed at each side of the pattern width (along the PP). At the left side of the rectangular units we have a distribution of poles pointing in one direction (up for example) with maximum signal or positive B_z , while at the opposite side (at the right) the poles are pointing downward, with minimum signal or negative B_z , as shown in Figure 2(c).

The magnitudes obtained by the simulations, 14.7 μT for S1 and 28.9 μT for S2, are consistent with the experimental results (S1 signal is 50% less than S2), which validates in a very good way our scanning process. On the calculations for S1, the amplitude has been calculated by an average of all the elements, taking into account that each row has different RD (if we simulate the magnetic component measured by S1 at the center of the 72 MTJ matrix, the amplitude is slightly lower: 13.5 μT). In the case of S2, the RD is the same in the 4 MTJ elements. Sensors S1 and S2 obtained experimentally the 75% and 90% of the simulated signal, respectively. These small differences between both methods could come from the approximation of the calculations or by a small misalignment of the scanning process (we must take into account that the sensors have approximately 30 μm of distance upon the edge of the chip); therefore currently we are working on tuning the procedures of both methods.

After analyzing the given results from both sensors for the CoCrPt media, and concluding that they match with the simulations, measurements of the ink were carried out. The simulation of the ink is not well controlled due to its nature: it is composed of particles with an inhomogeneous distribution in a solution over the paper, therefore it does not behave as a bulk ferromagnet; even when using the magnetization at 70 mT obtained from the MH loops, the signals obtained by both methods do not match thanks to the non-uniform dispersion of the particles. This is still under investigation.

First, studying the MH loops of one rectangular structure for each layer of magnetic ink on Figure 4a (where the magnitude of the field created by the permanent magnets is marked), we can

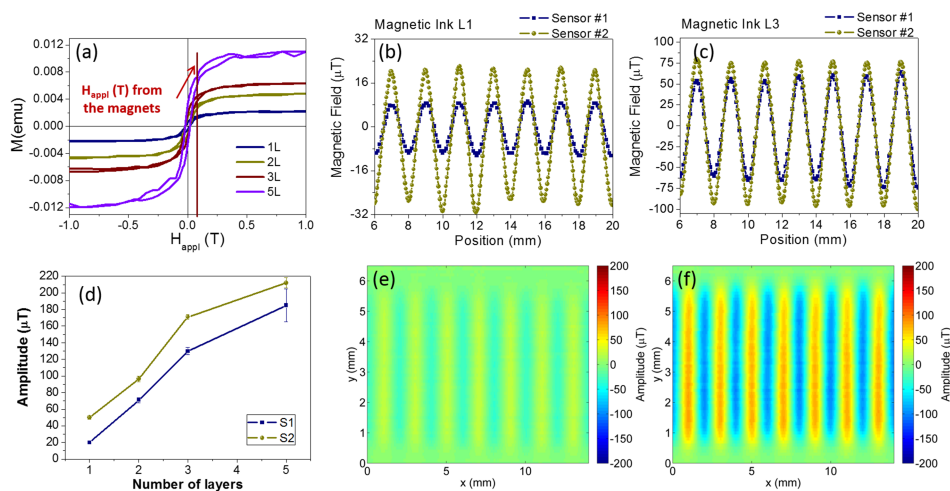


FIG. 4. L1 and L4: (a) Hysteresis loops, MH loops, of one rectangular structure of the magnetic ink with different thickness; (b) and (c) z-component of the magnetic signal from the S1 and S2 for L1 and L3; (d) Amplitudes vs layers; (e) and (f) Scan for L1 and L3 by S2.

observe that the increment of the magnetization (in emu) is linear with the thickness, which was expected. The unit of magnetization is in emu since the information about the printed volume is unknown, while the applied magnetic field is in T for comparison purposes with the permanent magnets. The magnetization of the printed ink during the scanning lies on the plane of the paper (although is not to fully saturated), causing, as in the CoCrPt media, uncompensated stay fields in the z direction. Figure 4(b) and (c) shows the amplitudes of the magnetic signal obtained by both sensors on L1 and L3 samples, and Figure 4(d) the amplitude vs. the number of layers. In the later we can observe how the signal increases with the number of layers in a proportional way. As expected, S2 has higher signal than S1, with good SNR on both cases. In L1 sample, S1 measured the 40% of the amplitude that S2 obtained, which is very similar as the CoCrPt case, but this percentage increases with thickness, being 75% and 76% for L2 and L3, respectively, reaching to an 87% in the L5 sample. This could be due to the fact that the increasing signal of the ink, improves the averaged signal of the 72 MTJ elements.

The 2D scan, Figure 4(e) and (f), shows as well the good spatial resolution of the scanning process. In this case we don't show the schemes of the rectangles as in Figure 3(a) and (b), but the stray fields have the same behavior, a uniform distribution along the long edge of the units. This scanning mapping, give us a hint about the magnetic particles distribution, which in these cases look very homogeneous. This is a good feedback to improve the analytical calculations of the magnetic particles of the ink.

In conclusion, a good MR sensor geometry or setup, to read small z -magnetic component signals produced by patterned magnetic ink and CoCrPt, was found; this setup includes two permanent magnets placed at an optimized distance from to the sensors, with high enough magnetic field to magnetize the patterns, without compromising the sensors performances. The patterns have 1 mm of PP, while the scanning was made at a RD of half PP, although higher distances are under test. Two different MTJs configuration were used, S1 with 72 elements in an array geometry, and S1 with 4 MTJs in a row with the same RD. In the former, lower amplitude were obtained due to the averaged signal from the elements with different RD. In the case of the CoCrPt media, both sensors achieved results that are in good agreement with the analytical calculations, validating their performances; in the case of S1, the experimental amplitude of the B_z signal is 75% of the simulated data, while S2 corresponds to the 90%. The differences from both methods can be decreased by improving the height control of the scanner, which is actually quite accurate; the z motion (vertical) of the scanner has a precision of 3.5 μm . The performance of this MR sensor setup is promising for future measurements at different RD, different PP or different magnetic particles.

ACKNOWLEDGMENT

This work was supported by the Project Tumapos (H2020-SME-INST-684491) and by the FCT scholarships SFRH/BD/111538/2015. The work of R. Ferreira and P. P. Freitas was supported by the IMAGIC EU-FP7-ICT project n°288381. The authors want to thank to D. C. Leitao by the magnetic discussions.

¹ S. Furrer *et al.*, *IEEE Transactions on Magnetics*.

² S. Iwasaki and K. Ouchi, *IEEE Trans. Magn.* **26**(1), 97–99 (1990).

³ N. Sekiguchi, T. Aizawa, H. Terui, T. Ozaki, H. Murakami, T. Endo, J. Tachibana, R. Hiratsuka, and S. Inoue, *IEEE Trans. Magn.* **50**(11) (2014), Art. ID 3202904.

⁴ Information Storage Industry Consortium (INSIC) 2015-2025 Tape Roadmap, <http://www.insic.org/news/2015%20roadmap/15pdfs/2015%20Technical%20Roadmap.pdf>.

⁵ "IBM Introduces the Industry's Fastest One Terabyte Storage Tape Drive", New release, July 15, 2008. Available online at: <http://www-03.ibm.com/press/us/en/pressrelease/24619.wss#release>.

⁶ INSIC's 2012-2022 International Magnetic Tape Storage Roadmap, <http://www.insic.org/news/2012Roadmap/12index.html>.

⁷ R. Ferreira, E. Paz, P. Freitas, J. Wang, and S. Xue, *IEEE Transactions on Magnetics* **48**, 3719–3722 (2012).

⁸ F. A. Cardoso, L. S. Rosado, F. Franco, R. Ferreira, E. Paz, S. F. Cardoso, P. M. Ramos, M. Piedade, and P. J. P. Freitas, *IEEE Trans. Magn.* **50**(11), 6201304 (2014).

⁹ B. Negulescu, D. Lacour, F. Montaigne, A. Gerken, J. Paul *et al.* (2009).

¹⁰ F. N. Hooge, T. G. M. Kleinpenning, and L. K. J. Vandamme, *Rep. Prog. Phys.* **44**, 479 (1981).

¹¹ H. N. Bertram, *Theory of Magnetic Recording* (Cambridge University Press, 1994).

¹² F. Franco, F. A. Cardoso, L. S. Rosado, R. Ferreira, S. Cardoso, M. Piedade, and P. P. Freitas, *IEEE Transactions on Magnetics* **53**(4) (2016).